Dynamic Elastic Modulus Variability in Anisotropic and Isotropic Materials: Comparison by Acoustic Emission

Henrique Pina Cardim, Larissa Queiroz Minillo, Fernando Nakao and Altibano Ortenzi*

State University of Londrina - CTU, Celso Garcia Cid Highway, km 380, Londrina, PR, Brazil

Abstract: This study compared the variation of the dynamic elastic modulus (E) of three types of composite pipes made by the filament winding process and a steel alloy specimen, according to signal source changes. The specimens were produced with three different winding angles, i.e., ±50°, ±52.5°, and ±55°. The moduli were obtained through a known signal source and the angular variation, according to two sensors positioned over the specimen's surface. In a previous article, the variation in the velocity of acoustic emission (AE) signals, performed in the same type of pipes, was discussed based on the standards for glass fiber-reinforced epoxy (GFRE) filament wound specimens. This work took these preliminary findings to compare with the results found for steel alloy pipes (SAE 1020). This data was used with appropriate equations to determine the dynamic elastic moduli of each material. It was found that, even for small angular differences, the modulus changes position concerning the lamination angle. Thus, the lower the quality control, the lower the final product with composite materials. As expected, for isotropic materials such as steel alloys, the modulus remains constant along the angles, while for anisotropic ones, it is dependent on the principal directions of stress and strain, or on the other hand, dependent on the correlation between the angular wave velocity of the AE signals.

Keywords: Composites, acoustic emission, dynamic elastic modulus, filament wound, pipes.

1. INTRODUCTION AND BACKGROUND

The constant growth of composite materials as structural members in many fields of engineering (nautical, aerospace, civil, and biomechanics), and the importance of damage prediction through the completely serviceable life of various structures assume an important role in the nondestructive evaluation methods. However, there are many uncontrollable variables concerning the use of composites. On one hand, the structural designer must know well how the structural member will work and then design the composite more fitted to solicitations over the member or structure. This procedure produces a sort of different materials, with different mechanical properties. Thus, for each design of great complexity is necessary to evaluate the typology of the composite that will be used. In contrast, structural members and components need their evaluation during their serviceable life, because of critical conditions of use environmental, seismic, or fatigue, which could cause injuries in humans [1-5]

The previous articles [6, 7] showed the behavior of the acoustic signals over filament wound composite pipes, and how the position of the signal source or, in this case, the damage occurrence could be interfered with by the interlacing of opposites filaments of roving, regarding the lamination path. Three types of specimens with three different winding angles, i.e., ±50°, ±52.5°, and ±55° were analyzed.

This paper presents the continuation of prior studies, which comprised the verification of the variation that occurred in the dynamic elastic modulus (E_{11}) regarding the three angular winding laminations described, in comparison with an isotropic material.

It is well known how the AE can find damage occurrences and crack propagation in composite materials [7-13], as so as the procedures to use the nondestructive technique [14-16] for evaluation of damage propagation, for numerous composites and plate structures [9, 11, 17, 18]. However, the literature presents scarce works on industrialized lamination processes evaluation, where the layering presents unusual directions like FW, the pultrusion, sheet molding compound (SMC), or automated fiber placement (AFP), which use unidirectional or bidirectional fabrics, or prepreg [19].

2. MATERIALS AND METHOD

A PC-based oscilloscope with a maximum resolution of 16 bits and frequency of 20 MHz per channel, with the ability to take four signals, at the same time, up to 10.0E6 samples per second. This equipment was chosen because of its flexibility and portability. Other similar instruments do not have four simultaneous channels integrated with software in a compact data acquisition system.

*Address correspondence to this author at the State University of Londrina - CTU, Celso Garcia Cid Highway, km 380, Londrina, PR, Brazil;
E-mail: ortenzi@uel.br

E-ISSN: 1929-5995/23

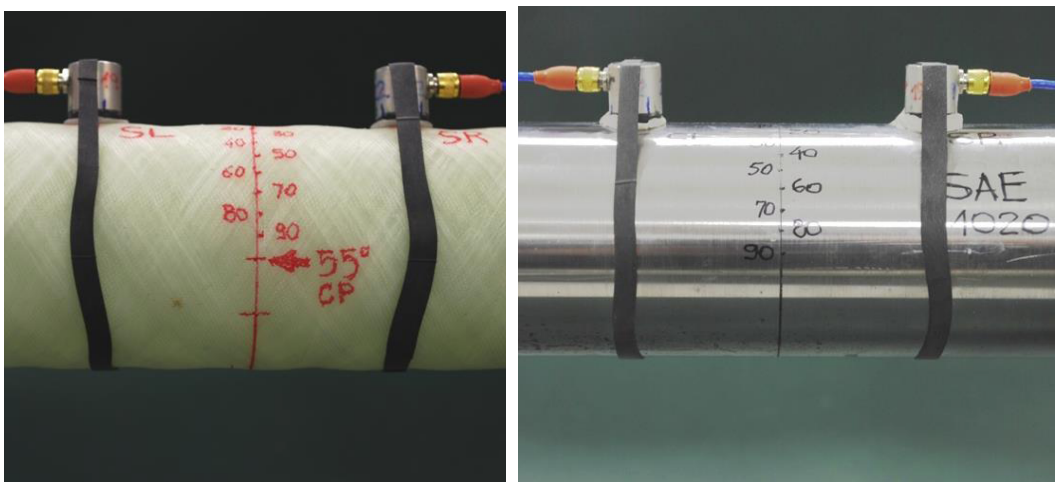

a b

Figure 1: Composite pipe (**a**), and SAE 1020 steel pipe (**b**) setups.

Two collinear DUNEGAN SE25-P sensors broadband with a flat response from 20 kHz up to 600 kHz were used.

The 'pencil lead break' or Hsu-Nielsen test is a simple standard procedure [15] to create a standard signal using a 0.3 mm mechanical pencil. The pencil is refueled with 2H leads. To prevent slippage or undesirable secondary noise because of small friction on the surface, the pencil is inserted in a fixture made of polyamide or silicon rubber, where only the lead appears on the opposite side.

Two supports in wood, covered with neoprene to isolate external noise in the specimen, were mounted over a rigid granite plate, to assure the isolation of any external vibration during the tests.

Figures **1a** and **b** show the position and fixture of the sensors for the composite and steel pipes, respectively.

All the specimens were marked according to Figure **1**, from zero degrees up to 90 degrees, with marks separated by ten degrees, one to another. For the composite pipes, one mark is made over the aligned position where theoretically the filaments are interlaced, as a function of the winding angle of each specimen. These marks are shown schematically in Figure **2**.

Figure **3a** shows the signals acquired from the sensor at the left side (SL) and (b) the signals acquired from the sensor at the right side (SR), respectively, for the specimen SP1 (±50°), with the intensity in dB plotted against the time in $3x10^{-3}$ s.

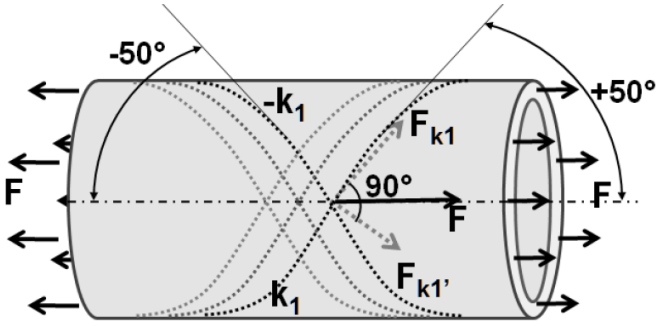

Figure 2: Theoretical marks of the filament path interlacing during the pipe production.

After the acquisition, the window is zoomed for each signal and, through the software, the rulers are positioned over the zero intensity, and the vertical ones are positioned over the peaks to measure the period and the time delay from the first and the second peaks. Then, the frequency is calculated. After, all results were organized on the spreadsheets, which were calculated for all averaged results regarding both sensors.

2.1. Modulus through Acoustic Emission Signal Acquisition

Studies in the literature [20, 21] show that it is possible to associate the wave speed with the mean in which they are propagated, and this is shown through Equations 1 to 6.

$$v = \sqrt{\frac{E}{\rho}} = v^2 = \frac{E}{\rho} \quad \text{(Eq. 1)}$$

Where:

v = acoustic signal velocity in the mean

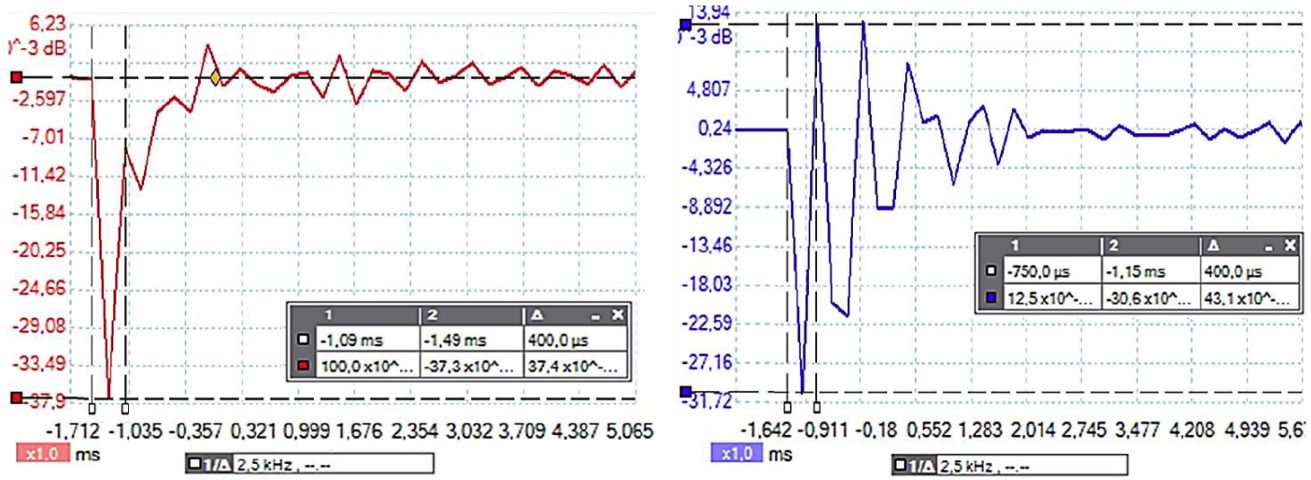

a **b**

Figure 3: Signals from SL (**a**), and signals from SR (**b**), for the SP1 wound in direction ±50°.

E = longitudinal elastic modulus

ρ = material density

By analysis of the units involved and the ratio contained in these properties can be obtained the following relations (either in consideration the initial space is equal to zero):

$$E = \frac{\sigma}{\varepsilon} = \frac{F * l}{l^2 * \Delta l} = \frac{m}{t^2 * \Delta l} \quad \text{(Eq. 2)}$$

Where:

σ = stress

ε = strain

l = some unit of length

t = some unit of time

m = some mass unit

Δl = total elongation, which can be taken as a final length less initial length

Taking the average space ratios and average speed from physics, and assuming that the initial space and the initial elongation are equal to zero, the ratio from Equation 2 can be transformed into Equation 3:

$$\frac{m/t^2 * l}{\rho} = \frac{m}{t^2 * l} * \frac{l^3}{m} = \frac{l^2}{t^2} = v^2 \quad \text{(Eq. 3)}$$

Where:

v = mean velocity

As seen, this ratio agrees with the ratio of Equation 2 above. However, this can be fully valid for homogeneous and isotropic media. In the case of non-homogeneous media, even if isotropic, or one or more anisotropic media, new considerations must be made. To consider the anisotropy in composites, Equation 2 was used. Thus, Equations 4 and 5 show the new ratio.

$$v_E = \sqrt{\frac{E_{12}}{\rho}} \quad \text{(Eq. 4)}$$

or still:

$$v_L = \sqrt{\frac{E}{\rho}\left[\frac{1-\nu}{(1+\nu)(1-2\nu)}\right]} \quad \text{(Eq. 5)}$$

Where:

E = longitudinal modulus

$\mathbf{v_L}$ = velocity associated with the longitudinal modulus

The same analogy can be used for the tangential or shear module, which can be found in Equation 6.

$$v_G = \sqrt{\frac{\rho}{G_{12}}} \quad \text{(Eq. 6)}$$

Where:

G_{12} = tangential shear modulus to direction 1-2

v_G = mean velocity in relation to the direction 1-2

The isotropic or anisotropic variation of the materials can interfere with the propagation velocity of

Table 1: Average Moduli through Tensile Tests

Winding Angle (±°)	Axial Stress (MPa)	Elongation (200mm)*	ε12 (mm/mm)	ε 21 (mm/mm)	E12 (Gpa)	SD-E12	E21 (Gpa)	SD-E21
50	5.34	0.05703	0.000285	0.000135	18.37	0.781	39.78	2.014
52.5	5.28	0.04477	0.000295	0.000101	18.41	0.960	52.30	2.437
55	5.24	0.04634	0.000232	0.000098	15.28	0.732	58.24	2.916

*useful length of specimens.

sound signals. Therefore, it is possible to correlate the velocity of the wave according to the moduli and the composite density.

Through the equations above, it was possible to verify the elastic modulus for the tests conducted and compare it with the theoretical model.

2.2. Modulus Variation According to the Lamination Angles

First, the design magnitudes of the axial force for each specimen were taken. These forces were then decomposed in terms of two radial forces acting perpendicularly and axially to the filament path, respectively. However, there were also two other decomposed forces acting transversally to the radials.

The first is directed away from the wall tangentially, and the other is directed transversally to the wall pipe. Unless the stress level is greater than the matrix crack limit, or loss of adhesion between the matrix and fibers, the load is perfectly transmitted between the fiber filaments through the polymeric matrix.

From these considerations, one can find the stress acting parallel to the winding path, formed by an imaginary elliptical cross-section. Thus, the same correlation can be used to verify that the angular variation regarding the axial load can reduce the modulus E_θ, where θ is the winding angle of each specimen. These decomposed forces act mainly tangentially through the plies of the laminate. The first is aligned with a 'k_1' roving filament path and is named F_{k1}. The second force is perpendicular to the same 'k_1', but misaligned with the opposite '-k_1', and is named F_{k1}.

As this type of lamination has many subsequent plies of roving that follow the constant path and angles, any global axial force F of tension or compression is decomposed into both forces, considering the ±θ angle of lamination.

Unless the winding angle is ±45°, the directional stresses are not coincident in both directions.

For the case of the ±50.0° winding angle, the $Fk_{1'}$ is oriented to -40° from the path '-k_1' corresponding to -50°, for instance, as shown in Figure **2**, Table **1** shows the stresses regarding the axial direction (cross-sectional area of the pipes), and in directions 2 (tangential), and 3 (radial) for the three typologies, in contrast with an isotropic material, like the SAE 1020 steel.

To start the calculus of the moduli, according to the premises above, Equation 7 was used to find the E_{11} local modulus, according to the results reached for the decomposed forces regarding the axial loading design.

$$E = \frac{F_\theta L}{A_\theta \delta} \quad \text{(Eq. 7)}$$

Where:

F_θ = applied force in the considered direction or decomposition

L= total length of a structural member

δ_θ = total elongation of selected winding angle

A_θ = cross-sectional area for selected winding angle

The decomposed forces are acting over an elliptical cross-sectional area because of the rotation of imaginary plan 'yz' up to the winding path, with a center on the Cartesian origin. This plan represents the cross-sectional area that contains the ±θ sliced geometry path. Equation 8 gives A_θ.

$$A_\theta = \pi\left[(XY) - (xy)\right] \quad \text{(Eq. 8)}$$

Where:

X and x = the x aligned radii (highest and lowest)

Y and y = the y aligned radii (highest and lowest)

θ = the winding angle

Table 2: Moduli through Tensile Tests in Correlation with Tangential Loads

Winding Angle (±°)	y (mm)	Y (mm)	x (mm)	X (mm)	A (mm²)	δ (mm)	E_{11} (GPa)	E_{12} (GPa)
50	80.03	74.81	50.55	57.31	2990.22	0.05703	38.85	18.42
52.5	73.94	72.31	50.56	57.37	2910.49	0.04477	52.13	18.35
55	70.31	69.79	50.55	57.17	2734.89	0.04634	58.29	15.29

By fixing X and x as the internal and external radii of the pipe to receive the changes of Y and y according to θ, and supposing the axis of rotation to be z, the length of y or Y can be found using Equation 9:

$$y_S = \sqrt{(x_S \tan\beta)^2 + x_S^2} \quad \text{(Eq. 9)}$$

Where:

y_s = the correspondent value, highest or lowest

x_s = the correspondent x value according to y searched

β = complementary angle of the winding angle θ.

1644-9665Therefore, using Equation 9 to find the value of y, and then substituting Equation 8, it is possible to find the inclined plan that forms the elliptical cross-sectional area for each angle. Then, substituting Equation 7, it is possible to find the Modulus for each angular variation. Table **2** shows the decomposed forces for the design load of the specimens and the moduli E_{11} and E_{12}, respectively.

2.3. Pencil Lead Break Test (or Hsu-Nielsen Test)

To conduct the experimental phase, after preparing the specimens and devices, the pencil lead was broken five times, consecutively, over the same mark on the pipe, totaling 15 lead breaks by specimen typology, by angular variation.

For each angle, which is considered exactly symmetrically, the path from the sensors to the angle of interest was calculated, according to Equations 10 and 11. This was the procedure used to find the geodetic distance (or any curve C) between the sensors and the mark, represented by one half of a parabola, which starts at A (x,y,z) and ends at B (x,y,z). It does not mean the fiber path, but the probable path for some wound filament that passes through the same imaginary shortest path of wave propagation.

$$\oint f(x,y)\,ds = \int_a^b f\left(x(t), y(t), z(t)\right)\left|r'(t)\right|dt \quad \text{(Eq. 10)}$$

Where:

$$\left|r'(t)\right| = \sqrt{[x'(t)]^2 + [y'(t)]^2 + [z'(t)]^2} \quad \text{(Eq. 11)}$$

With **r'** corresponding to a vectored function in the subspace in R³.

By numerically integrating through tridimensional vectors and developing in terms of 'x', 'y', and 'z', the length of the curve can be found if the function is continuous and defined on an opened interval a-b. After some algebraic manipulation, for the particular case where the functions can be parabolic, elliptical, or geodetic and always finite and smooth, the problem can be reduced to the bi-dimensional Cartesian case of x-y, after rectifying the cylinder in a plane with the same measurements, and their distances can be calculated by vector sum. All measurements were performed in the same environmental condition, to avoid the effects of temperature and relative humidity (RH) variations on the specimens. The control was done with a thermo-hygrometer and with the air conditioning in the testing room. Table **3** shows the condition under which the tests were conducted. The same procedure described in this topic was used on the steel alloy specimen. Hence, more than 50 points were acquired for 10 angular variations in the steel pipe, except the C_P point. Table **3** shows the average results achieved for the PLB tests. Where the terms $AE_{\pm xx.x}$ refer to the three typologies of pipes used in the experiment. The subscripts '±xx.x' represent the winding angles.

3. RESULTS AND DISCUSSION

After compiling all data as described, the three tests were grouped, as shown in Table **4**, to compare their velocities according to angles, which presented the average results achieved for the 15 replications of the PLB test, for each angular variation.

A pattern can be visualized for the change in velocities. The SP1 (50°), SP2 (52,5°), and SP3 (55°) groups presented their lowest velocities for angles of 40°, 30° and 20°, respectively.

The difference between the lowest and the highest velocity was more than four times. The group with the lowest variation and lowest wave velocity was SP2. In contrast, the SP3 group presented the highest velocity.

Table 3: Results Achieved Using the PLB Tests for the 11 Replications for Each Typology [7]

Winding Angle (±°)	AE±50.0 (GPa)	SD ±50.0	AE±52.5 (GPa)	SD ±52.5	AE±55.0 (GPa)	SD ±55.0
0	9.446	0.475	8.603	0.429	10.219	0.489
10	11.897	0.598	6.377	0.318	3.730	0.179
20	14.669	0.737	6.273	0.313	3.633	0.174
30	3.246	0.163	4.559	0.227	3.981	0.191
40	2.967	0.149	13.119	0.654	9.747	0.467
Cp-50	53.468	2.686	18.667	0.931	24.521	1.174
Cp-52.5	26.967	1.355	42.782	2.134	37.943	1.817
Cp-55	17.061	0.857	29.204	1.457	49.726	2.382
60	6.469	0.325	17.483	0.872	6.951	0.333
70	4.202	0.211	16.580	0.827	7.086	0.339
80	11.867	0.596	14.859	0.741	5.325	0.255
90	10.061	0.505	9.034	0.451	17.108	0.819

Table 4: Compared Dynamic Moduli for Composite and Steel Pipes

Winding Angle (±°)	Typology						SAE 1020 (GPa)	Avg. SAE 1020	SD SAE 1020
	Avg. 50 (GPa)	SD 50	Avg. 52.5 (GPa)	SD 52.5	Avg. 55 (GPa)	SD 55			
0	4.03	0.16	3.67	0.16	4.36	0.21	208.04	±213.54	±7.67
10	6.30	0.25	3.38	0.15	1.98	0.10	201.86		
20	7.66	0.30	3.27	0.15	1.90	0.09	213.25		
30	2.53	0.10	3.55	0.16	3.10	0.15	214.40		
40	2.47	0.10	10.91	0.49	8.11	0.40	222.70		
50	39.13	1.53	14.78	0.66	19.15	0.94	211.86		
52.5	21.35	0.83	31.31	1.40	27.77	1.36	214.98		
55	13.32	0.52	22.80	1.02	36.39	1.79	218.10		
60	5.29	0.21	14.29	0.64	5.68	0.28	226.25		
70	3.26	0.13	12.85	0.57	5.49	0.27	199.68		
80	10.21	0.40	12.78	0.57	4.58	0.22	213.71		
90	10.06	0.39	9.03	0.40	17.11	0.84	217.69		

After the results obtained through the preliminary studies, they were used to calculate the longitudinal elastic modulus (E_{11}), after using the equations described above, for ten angular variations, and for each dynamic modulus obtained through the signal waves.

It was found that using the amplitude correction coefficients, the increase and reduction of the dynamic modulus accompanies the more coherently and proportional angulation, for all typologies of **SPs**, while by using equations related to speed, for the case composites, the results are not proportional to angular variations. Equations 12 and 13 show the procedure.

$$E(v) = v^2\rho \rightarrow E_N(v) = v^2\rho\, C_{Anorm} \quad \text{(Eq. 12)}$$

$$E_{Test} = \frac{\sigma}{\varepsilon} \rightarrow E_{Test\,N} = \frac{\sigma}{\varepsilon} C_{Anorm} \quad \text{(Eq.13)}$$

Where:

E_N = elastic modulus.

$E_{Test\ N}$ = normalized elastic modulus achieved by the results for the stress-strain tests

C_{Anorm} = normalized amplitude coefficient, which is applied as a correction factor

The materials and the means were maintained invariably for all the specimens. The matrix phase and the fiber one are the same for the three typologies. Therefore, only the winding angle changed, which may have caused fiber slippage during the manufacturing process. However, for this study, the specimens were considered well done without misalignment and the presence of voids.

Regarding the results achieved, higher velocities were achieved when the signal source was positioned over the C_P position. In addition, the alignment of the fibers provided the gain in velocity, probably because of the accumulation of fibers and the reduction in matrix percentage in this direction.

To verify this condition, the better way will be to verify the transverse sectional area by scanner electronic microscopy (SEM). Yet, the results presented some coherent values regarding the angular positions, mean velocity, and angular frequency by the group.

Table **4** shows the results of the elastic dynamic moduli in the various directions of the laminate and the comparison with elastic moduli of steel, from the resulting velocities of the PLB [7] test, after the application of intermediate results on Equations 4 to 12 above, for each typology of composite pipe, and for the SAE 1020 pipe. Table **4** shows the great variation of modules for the FW SPs, according to the wave incidence regarding the C_P (values typed in bold), in which the signal wave is parallel to the last ply of roving bands.

For all the average results achieved (shown in Tables **1**, **3**, and **4**) the standard deviation (SD) remained between ±3.9 and ±5.3%. Thus, it is possible to infer that the results were satisfactory concerning the variability of the 11 replications of PLB.

On the steel pipe, the variation was about ±7.7%, although the steel is considered a homogeneous material. This variation could be derived from the pencil point small movements in each repetition, over a less rough surface than the composite ones.

For each angular variation, it is remarkable that the values decrease when the PLB application angle decreases or increases, referring to the C_P position. This phenomenon can be explained by the alternating plies at opposite angles (±x), which form the thickness of the filament wound pipes. The latter is formed by 16 alternating paths to complete eight equivalent layers or plies. Therefore, the first layer remains in the +X° direction, while the subsequent layer is applied in the -X° direction, alternatively, when completing the pipe thickness along the full length of the mandrel.

Unless expected, the increase was not due to the remoteness of the signal in relation to the C_P angles. This effect should be investigated at opposite angles and their bisector to verify whether the phenomenon is repeatable and whether it can be considered a pattern for other angular variations.

In the SAE 1020, there was a variation in elastic dynamic modulus of 13.3% between the lowest and highest value, and this discrepancy can be caused by minor variations in the pencil lead positioning, which was done manually. Probably, with a mechanical PLB system, this difference will not appear.

Figure **4** indicates the distribution of modules according to angular variations, compared to the SAE 1020 pipe.

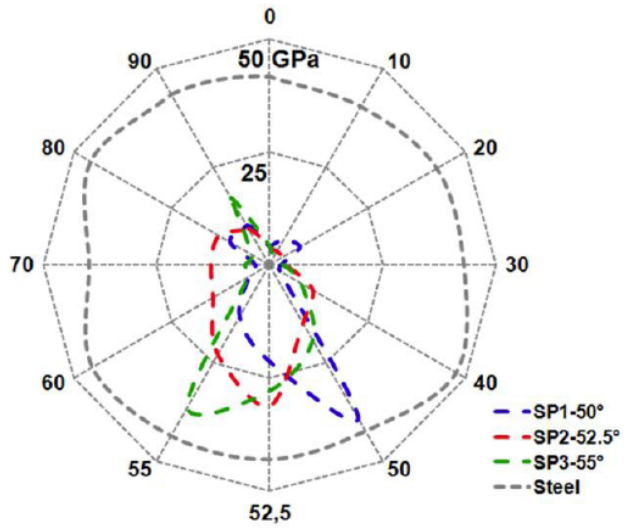

Figure 4: Compared Moduli distribution between composite and steel pipes.

It is emphasized that the values are not scaled, giving only a qualitative behavior of the elastic dynamic modulus variation of the filament wound pipes, in comparison with the quasi-linear behavior of the steel pipe.

It is possible to assume that the low values are derived from the layers which are in the opposite direction, symmetrical, in addition to the irregularity

between the two phases that do not obey the absolute parallelism, in the laminated plane.

To investigate these hypotheses, other further verification would be necessary, such as the use of tomography or other techniques to map a three-dimensional sample and calculate these variations accurately to correlate them with the results obtained here.

4. CONCLUSION

AE is a widely applied method on steel pressure vessels and other steel structures to predict damage. When the material changes from isotropic to anisotropic, there are problems. The complexity of the microstructure in these materials is great and the ability to build structures oriented towards the maximum performance of the material. However, to improve the knowledge about the damage behavior of the fiber-reinforced polymer, the AE technique is cost-effective and, unlike others, it can be used continuously at the operating site of an observation limb.

Regarding the study conducted by this experimental procedure, it is possible to use, with certain criteria, the results obtained for velocity variation in anisotropic mean.

As noted, the speed is theoretically invariant in an isotropic environment (PLB test in steel), and takes into account a perfectly homogeneous material, without insertions or discontinuities at the microscopic level. In polymeric composites, which are anisotropic by the constitution, it is dampened in part by the variation in the density of the medium and part by differences in fiber orientation, also discounting microscopic and macroscopic imperfections, which are more influential in the results.

REFERENCES

[1] Cortés G, Suarez E, Gallego A, *et al*. Health monitoring of reinforced concrete structures with hysteretic dampers subjected to dynamical loads by means of the acoustic emission energy. Struct Heal Monit 2019; 18: 1836-1850. https://doi.org/10.1177/1475921718813489

[2] Du F, Li D, Shan B, *et al*. Failure behavior monitoring and evaluation of steel-confined reinforced concrete columns by acoustic emission under quasi-static loading. Lat Am J Solids Struct; 15. Epub ahead of print 24 October 2018. https://doi.org/10.1590/1679-78255170

[3] Bertetto AM, Masera D, Carpinteri A. Acoustic emission monitoring of the turin cathedral bell tower: Foreshock and aftershock discrimination. Appl Sci; 10. Epub ahead of print 1 June 2020. https://doi.org/10.3390/app10113931

[4] Świt G. Acoustic Emission Method for Locating and Identifying Active Destructive Processes in Operating Facilities. Appl Sci 2018; 8: 1295. https://doi.org/10.3390/app8081295

[5] de Oliveira BCF, Nienheysen P, Baldo CR, *et al*. Improved impact damage characterisation in CFRP samples using the fusion of optical lock-in thermography and optical square-pulse shearography images. NDT E Int; 111. Epub ahead of print 1 April 2020. https://doi.org/10.1016/j.ndteint.2020.102215

[6] Ortenzi ACJCA, de Carvalho J, Corvi A. Comparison Behavior of Tensile Tests for GFRP Filament Wound Pipes With Two Different Sectional Areas Regarding High Temperature. Pipeline Riser Technol 2012; 3: 955. https://doi.org/10.1115/OMAE2012-84256

[7] Ortenzi A, Corvi A, Virga A. Preliminary study on the acoustic emission wave velocity on filament wound glass fiber reinforced polymer pipes and its correspondence with the winding angle. 2014. Epub ahead of print 2014. https://doi.org/10.4028/www.scientific.net/AMR.891-892.1243

[8] Maguire JR. Acoustic emission monitoring of composite containment systems. J Phys Conf Ser 2011; 305: 149-158. https://doi.org/10.1088/1742-6596/305/1/012044

[9] Suresh Kumar C, Arumugam V, Santulli C. Characterization of indentation damage resistance of hybrid composite laminates using acoustic emission monitoring. Compos Part B Eng 2017; 111: 165-178. https://doi.org/10.1016/j.compositesb.2016.12.012

[10] Chou HY, Mouritz AP, Bannister MK, *et al*. Acoustic emission analysis of composite pressure vessels under constant and cyclic pressure. Compos Part A Appl Sci Manuf 2015; 70: 111-120. https://doi.org/10.1016/j.compositesa.2014.11.027

[11] De Rosa IM, Santulli C, Sarasini F. Acoustic emission for monitoring the mechanical behaviour of natural fibre composites: A literature review. Compos Part A Appl Sci Manuf 2009; 40: 1456-1469. https://doi.org/10.1016/j.compositesa.2009.04.030

[12] Azadi M, Alizadeh M, Jafari SM, *et al*. Cumulative acoustic emission energy for damage detection in composites reinforced by carbon fibers within low-cycle fatigue regime at various displacement amplitudes and rates. Polym Polym Compos 2021; 29: S36-S48. https://doi.org/10.1177/0967391120985709

[13] Šofer M, Cienciala J, Fusek M, *et al*. Damage analysis of composite cfrp tubes using acoustic emission monitoring and pattern recognition approach. Materials (Basel) 2021; 14: 1-16. https://doi.org/10.3390/ma14040786

[14] ASTM International. Standard Practice for Acoustic Emission Examination of Reinforced Thermosetting Resin Pipe (RTRP) 1. Society 2001; 97: 1-4.

[15] ASTM International. Standard Guide for Determining the Reproducibility of. 2009. Epub ahead of print 2009.

[16] ASTM International. Standard Practice for Acoustic Emission Examination of Fiberglass Reinforced Plastic Resin (FRP) Tanks / Vessels 1. 2009; 1-15.

[17] Rojek M, Stabik J, Sokół S. Fatigue and ultrasonic testing of epoxy-glass composites. J Achiev Mater Manuf Eng 2007; 20: 183-6.

[18] Diakhate M, Bastidas-arteaga E, Moutou R, *et al*. Cluster analysis of acoustic emission activity within wood material : Towards a real-time monitoring of crack tip propagation. Eng Fract Mech 2017; 180: 254-267. https://doi.org/10.1016/j.engfracmech.2017.06.006

[19] Ngo SI, Lim Y Il, Hahn MH, *et al*. Prediction of degree of impregnation in thermoplastic unidirectional carbon fiber prepreg by multi-scale computational fluid dynamics. Chem Eng Sci 2018; 185: 64-75. https://doi.org/10.1016/j.ces.2018.04.010

[20] Bohse J. Acoustic emission characteristics of micro-failure processes in polymer blends and composites. Compos Sci Technol 2000; 60: 1213-1226. https://doi.org/10.1016/S0266-3538(00)00060-9

[21] Ni QQ, Iwamoto M. Wavelet transform of acoustic emission signals in failure of model composites. Eng Fract Mech 2002; 69: 717-728. https://doi.org/10.1016/S0013-7944(01)00105-9

Received on 02-01-2023 Accepted on 05-02-2023 Published on 09-03-2023

https://doi.org/10.6000/1929-5995.2023.12.01